

**WIDEBAND DIELECTRIC FEEDER FOR K-BAND PARABOLIC
ANTENNA**

by

IHSAN BIN AHMAD ZUBIR

**Thesis submitted in fulfilment of the
requirements for the degree of
Doctor of Philosophy**

July 2018

ACKNOWLEDGEMENT

In the name of Allah, the Most Gracious and Most Merciful. My greatest thank to Allah the Almighty for the blessing and guidance, with His willing, I was able to complete my master thesis. All praise belongs to Him.

I would like to express my genuine gratitude to both my dedicated supervisors Professor Ir. Dr. Mohd Fadzil Ain and Professor Zainal Arifin Ahmad for their support and encouragement during the period of my studies. Your practical view and guidance on my research work was of the utmost important. Thank you very much for the unending help throughout the course of my research.

To my dearest wife, Khadijah binti Md Noh, my beloved children, Hannan and Muhammad Bilal, thank you for your everlasting love, endless moral support, care, patient, prays and always being there for me when I need you most. Special dedication to my beloved parents, Ahmad Zubir bin Abdul Rani, and Laily Fauziah bt Hashim, my parents in law, my brothers and sisters, thanks for your everlasting prays and support. My best regards to Ministry of Higher Education for granting me the Mybrain (MyPhD) scholarship to assist financially for my study.

Last but not least, I would like to address my gratitude to members of my research group; Dr Asari Sulaiman, Dr Ali Othman, Dr Yazeed Qasaymeh, Dr Seyi, Dr Wan Fahmin Faiz, Dr Nik Akmar Rejab, Dr Mohd Azman Zakariyya, Dr Kang Chia Chao, Dr Ubaid Ullah, Khairul Anuar, Muhammad Fathul Najmi and Zulaimi Zahar, all the staffs and assistant engineers of School of Electric and Electronic Engineering and School of Material and Mineral Resources Engineering of USM, especially to Mr. Abdul Latip Hamid, Mr Elias Zainuddin and Mdm Zammira Khairuddin, for their cooperation and assistance. And also to all people that contributed their helps

directly and directly, thank you so much and all your contribution will not be forgotten.

TABLE OF CONTENT

	Page
ACKNOWLEDGEMENT	ii
TABLE OF CONTENTS	iv
LIST OF TABLES	viii
LIST OF FIGURES	ix
LIST OF SYMBOLS	xiv
LIST OF ABBREVIATIONS	xvi
ABSTRAK	xviii
ABSTRACT	xx
CHAPTER ONE: INTRODUCTION	
1.1 Introduction	1
1.2 Problem Statement	3
1.3 Research Objectives	5
1.4 Organization of the Thesis	6
CHAPTER TWO: LITERATURE REVIEW	
2.1 Introduction	7
2.2 Parabolic Antenna	7
2.2.1 Parabolic Antenna Operating Principle	7
2.2.2 Antenna Feeder	8
2.2.3 Gain and Efficiency	16
2.2.4 Beamwidth	17
2.3 Dielectric Resonator Antennas	17
2.4 Characteristics of DR	18

2.4.1	Dielectric Permittivity	18
2.4.2	Quality Factor	18
2.4.3	Bandwidth	19
2.4.4	DRA Fabrication Issues	19
2.5	Cylindrical DRA	19
2.6	Half Cylindrical DRA	22
2.7	Bandwidth Enhancement Techniques	26
2.7.1	Stacked	29
2.7.2	Perforated Technique	35
2.8	Summary	42
 CHAPTER THREE: METHODOLOGY		
3.1	Introduction	44
3.2	The Design Specification	46
3.3	Simulation Step Using CST	47
3.4	Fabrication of Dielectric Materials	50
3.4.1	Synthesize of MgZrO ₃ Compound	50
3.4.2	Pressing of Dielectric Materials	51
3.4.3	Sintering	52
3.4.4	Characterization of the Sintered Dielectric Materials	52
3.5	Hardware Preparation	55
3.6	Measurements of the Antenna	56
3.6.1	Dielectric Resonator Antenna Measurement	56
3.6.2	Parabolic Antenna Measurement	60
3.7	Summary	62

CHAPTER FOUR: PARABOLIC ANTENNA DESIGN AND APPROACH

4.1	Introduction	63
4.2	Principle of Feeding Mechanism	63
4.3	Design of a Rectangular Slot of Dielectric Resonator Antenna (DRA)	65
4.3.1	Estimation of Aperture Slot Length and Width	66
4.4	Design of Stacked Perforated Dielectric Resonator Antenna (SPDRA)	67
4.4.1	Determination of The Diameter of Stacked Cylindrical DRs	68
4.4.2	Perforated Stacked Cylindrical DRs Structure	69
4.4.3	Parametric Study on Stacked Perforated Dielectric Resonator Antenna (SPDRA)	71
4.4.4	Simulation and Measurement Result of SPDRA	83
4.5	Design of Stair Shaped Half Cylindrical Dielectric Resonator Antenna (SHCDRA)	89
4.5.1	Determination of the Diameter of Stacked Cylindrical DRs	90
4.5.2	Stair Shaped Half Cylindrical Dielectric Resonator Structure	91
4.5.3	Parametric Study on Stair Shaped Half Cylindrical Dielectric Resonator Antenna (SHCDRA)	92
4.5.4	Simulation and Measurement Results of SHCDRA	103
4.6	Comparison between SPDRA and SHCDRA Performance	108
4.7	Parabolic Antenna Design	109
4.8	Summary	111

CHAPTER FIVE: RESULT AND DISCUSSION

5.1	Introduction	112
5.2	Dielectric Materials Analysis	112
5.2.1	XRD Analysis	112

5.2.2	FESEM Analysis	113
5.2.3	Permittivity and Loss Tangent	114
5.3	Parabolic Antenna with SPDRA as a Feeder	115
5.3.1	3D Radiation Pattern	115
5.3.2	Measured and Simulated Radiation Pattern	116
5.4	Parabolic Antenna with SHCDRA as A Feeder	121
5.4.1	3D Radiation Pattern	120
5.4.2	Measured and Simulated Radiation Pattern	121
5.5	Summary	126

CHAPTER SIX: CONCLUSION AND RECOMMENDATIONS

6.1	Conclusion	128
6.2	Recommendations	129

REFERENCES	130
-------------------	------------

APPENDICES

Appendix A: Matlab Code for DRA Design

Appendix B: RO4000 Laminates – Data Sheet

Appendix C: Radiation Pattern and Gain Measurement

Appendix D: Measured Return Loss

Appendix E: Measured Radiation Pattern

Appendix F: Characterization Result of ϵ_r for Dielectric Resonator

LIST OF PUBLICATIONS

LIST OF TABLES

	Page
Table 2.1: Summary of measured hat feed with enhanced impedance bandwidth	15
Table 2.2: Summary of measured DRAs with enhanced impedance bandwidth	27
Table 3.1: Specification of parabolic antenna	46
Table 3.2: Compositions to produce 100 gm of MgZrO ₃ compound	50
Table 4.1: Constant parameters with different length slot, L_s	73
Table 4.2: Constant parameters with different stacked arrangement	75
Table 4.3: Operating band of SPDRA based on the stack order	77
Table 4.4: Constant parameters with different numbers of holes	79
Table 4.5: Constant parameters with different diameter of holes	80
Table 4.6: Optimum design parameters of SPDRA	83
Table 4.7: Constant parameters with different stacked arrangement	94
Table 4.8: Operating band of SPDRA based on the stack order	96
Table 4.9: Constant parameters with different thickness of DRs, h	97
Table 4.10: Constant parameters with different slot length, L_a	99
Table 4.11: Constant parameters with different rotation angle, θ^0	100
Table 4.12: Frequency range and bandwidth of SHCDRA with different rotation angle	100
Table 4.13: Dimensions of optimized parameters for SHCDRA	101
Table 4.14: Measured gain of the DRA feeder designs	109
Table 5.11: Dimensions of optimized parameters for SPDRA	108
Table 5.1: Simulation and measurement results of radiation pattern of parabolic antenna with SPDRA as feeder	116
Table 5.2: Simulation and measurement results of radiation pattern of parabolic antenna with SHCDRA as feeder	122
Table 5.3: Measured gain and maximum 3dB HPBW of the DRA feeder	127

LIST OF FIGURES

	Page
Figure 2.1: A paraboloid enables wavefronts to combine and not be out of phase	8
Figure 2.2: Front or axial feed	9
Figure 2.3: Offset axis feed	10
Figure 2.4: Cassegrain feed	10
Figure 2.5: Gregorian feed	11
Figure 2.6: Hat feed with corrugated brim (hat), dielectric support (head) and waveguide (neck)	12
Figure 2.7: Configuration of a stacked patch pyramidal horn antenna	12
Figure 2.8: Pyramidal horn antenna fed by planar antennas: (a) Bow-tie dipole; (b) Vivaldi	13
Figure 2.9: Horn antenna excited by microstrip patch configuration	13
Figure 2.10: Hat feed with corrugated brim (hat), dielectric support (head) and waveguide (neck)	14
Figure 2.11: The working principle (a) no corrugation introduced on hat, (b) corrugation introduced on hat	15
Figure 2.12: Various DR geometries	18
Figure 2.13: Cylindrical DRA geometry on metallic ground plane	20
Figure 2.14: Field distribution of the $TM_{01\delta}$ mode: (a) DRA field H_x and H_y at $z = 0$; (b) DRA fields E_y and E_z at $x = 0$	20
Figure 2.15: Field distribution of $HEM_{11\delta}$ mode: (a) DRA field H_x and H_y at $z = 0$; (b) DRA fields E_y and E_z at $x = 0$	21
Figure 2.16: Different excitation techniques of DRA: (a) Coaxial probe, (b) Slot-microstrip, (c) Microstrip, (d) Slot-waveguide, (e) Slot-image and (f) Image guide	21
Figure 2.17: Geometry of (a) Cylindrical and (b) Half-cylindrical DRA	23
Figure 2.18: Structure of the DRA (a) half cylinder and (b) half rectangular	24
Figure 2.19: Geometry of the DRA	25
Figure 2.20: 3D- view (a) Proposed cylindrical DRA and (b) Proposed half-	25

split cylindrical DRA

Figure 2.21:	Geometry of two element half split CDRA (a) side view and (b) top view	26
Figure 2.22	Dual band and wideband characteristic for two-DRA configuration (a) Dual bands: $(\Delta f_u + \Delta f_l) = 2(f_u - f_l)$ (b) Dual bands: $(\Delta f_u + \Delta f_l) < 2(f_u - f_l)$ and (c) Wideband: $(\Delta f_u + \Delta f_l) > 2(f_u - f_l)$	30
Figure 2.23:	Geometry of the stacked RDRA	31
Figure 2.24:	Stacked cylindrical DRAs (a) top view and (b) side view	32
Figure 2.25:	Structure of the proposed stacked DRA antenna	32
Figure 2.26:	(a) Exploded 3-D view of the DRA configuration and (b) Equivalent DRA	34
Figure 2.27:	Configuration DRA composed of two planar dielectric layers with different permittivities and (b) Feeding circuit of the microstrip-coupled slot	34
Figure 2.28:	The antenna design (a) Top view and (b) Side view	35
Figure 2.29:	Square hole lattice configuration	37
Figure 2.30:	The top view construction of quad-band perforated RDRA with single ceramic sheet with $\epsilon_r = 10.2$, $R_1 = 1.5$ mm, $S_1 = 2.085 R_1$, $R_2 = 1.2$ mm, $S_2 = 2.378 R_2$, $R_3 = 1.5$ mm, and $S_3 = 2.88 R_3$	37
Figure 2.31:	(a) Isometric view and (b) Front view of pierced rectangular DRA	38
Figure 2.32:	Rectangular Dielectric Resonator Antenna (RDRA) perforated with symmetrical array of square slots	40
Figure 2.33:	Top view of perforated minkowski fractal dielectric resonator antenna	40
Figure 2.34:	Perspective view of perforated RDRA without ground plane	41
Figure 2.35:	The symmetrical array of holes	41
Figure 2.36:	The cheeseholes type HDRA as viewed from different planes. (a) x-z plane, and (b) x-y plane	42
Figure 3.1:	Research Methodology Flowchart	45
Figure 3.2:	Waveguide port of DRA	48
Figure 3.3:	Parabolic antenna model in CST (a) Front view (b) 3D view	49

Figure 3.4:	Boundary condition of parabolic antenna	49
Figure 3.5:	Calcination profile for $MgZrO_3$	51
Figure 3.6:	Sintering profile for Al_2O_3 , SiO_2 and $MgZrO_3$	52
Figure 3.7:	Measurement setup of Dielectrics for characterization using 85070E Dielectric Probe Kit and Network Analyzer	54
Figure 3.8:	Dielectric probe calibration a) air; b) short; and c) water	54
Figure 3.9:	Parabolic antenna physical existing model a) front view, b) back view and c) hat feed	55
Figure 3.10:	Parabolic antenna physical existing model a) front view, b) back view	56
Figure 3.11:	S-parameter measurement using PNA-X Network Analyzer	57
Figure 3.12:	Instrument setup for radiation pattern and gain measurement for DRA in anechoic chamber at Penang Skill Development Center (PSDC)	59
Figure 3.13:	Placement of AUT for radiation pattern and gain measurement in anechoic chamber in E-plane and H-plane	59
Figure 3.14:	The configuration of a CATR	61
Figure 3.15:	Instrument setup for radiation pattern and gain measurement for parabolic antenna in anechoic chamber	62
Figure 4.1:	Length of microstrip line for the proposed DRA	65
Figure 4.2:	Rectangular slot located at the DRA centre (a) Top view, (b) Side view and (c) Geometry of rectangular slot	66
Figure 4.3:	Isometric view. (a) Solid cylindrical stacked DRs and (b) Perforated stacked DRs	69
Figure 4.4:	Geometry of stacked perforated DRs	70
Figure 4.5:	Perforated DR with square lattice. (a) Full unit cells of lattices and (b) A unit cell of lattice	71
Figure 4.6:	Simulated return loss with different values of slot's length	74
Figure 4.7:	Simulated return loss with different DR stacked arrangement	76
Figure 4.8:	DRs position in the middle of the slot (a) Front view and (b) Back view	79
Figure 4.9:	Simulated absolute electrical field at different frequency (a)	79

	14.08 GHz, (b) 19.45 GHz, (c) 22.68 GHz, and (d) 26.05 GHz	
Figure 4.10:	Simulated return loss when varying the numbers of holes	80
Figure 4.11:	Simulated return loss with different diameter sizes of 21 holes	81
Figure 4.12:	The comparison of simulated return loss with holes and without holes	81
Figure 4.13:	Geometry of SPDRA (a) Front view, (b) Side view and (c) Isometric view of stacked DRs	82
Figure 4.14:	Electrical distribution of resonant modes (a) 14.075 GHz, (b) 19.45 GHz, (c) 22.675 GHz, and (d) 26.05 GHz	83
Figure 4.15:	The simulated radiation efficiency of SPDRA	84
Figure 4.16:	The simulated VSWR of SPDRA	84
Figure 4.17:	Photograph of the fabricated hybrid stacked DRA. (a) Front view (b) Back view	85
Figure 4.18:	Simulated and measured return loss of the optimized SPDRA	86
Figure 4.19:	Simulated and measured radiation pattern of SPDRA in E- and H-planes at (a) 13 GHz, (b) 15 GHz, and (c) 18 GHz	89
Figure 4.20:	Simulated and measured gain of SPDRA	90
Figure 4.21:	Evolution of the proposed DRA in 3D view. (a) Cylindrical stacked DRs. (b) Half-cylindrical stacked DRs. (c) Stair-shaped DRs	90
Figure 4.22:	The arrangement of stacked half cylindrical resonators	91
Figure 4.23:	Illustration of magnetic field distribution in the proposed of SHCDRA	93
Figure 4.24:	Isometric view of half cylindrical DRA with stacked HCDR on the rectangular slot	95
Figure 4.25:	Simulated return loss with different DR stacked arrangement	96
Figure 4.26:	Simulated reflection coefficient when varying the thickness of DRs	98
Figure 4.27:	Rectangular slot of the DRA	99
Figure 4.28:	Simulated return loss when varying the rectangular slot length	99
Figure 4.29:	Stacked half cylindrical DRs rotation angle, θ_0	99
Figure 4.30:	Simulated return loss when varying the rotation angles of DRs	100

Figure 4.31:	Geometry of SHCDRA (a) Front view, (b) Back view and (c) Isometric view of stacked half DRs	101
Figure 4.32:	Simulated radiation efficiency of SHCDRA	102
Figure 4.33:	The simulated VSWR of SHCDRA	102
Figure 4.34:	Photograph of the fabricated hybrid stacked SHCDRA. (a) Front view (b) Back view	103
Figure 4.35:	Simulated and measured return loss of the optimized SHCDRA	104
Figure 4.36:	Simulated rotation angle +/-10% tolerance of the SHCDRA	105
Figure 4.37:	Simulated and measured radiation pattern of SHCDRA in E- and H-planes at (a) 13 GHz, (b) 15 GHz and (c) 18 GHz	107
Figure 4.38:	Measured and simulated gain of the proposed SHCDRA	108
Figure 4.39:	Geometry of parabolic reflector	110
Figure 5.1:	XRD pattern of Al ₂ O ₃ , MgZrO ₃ and SiO ₃	114
Figure 5.2:	FESEM images of (a) Al ₂ O ₃ , (b) SiO ₃ , (c) MgZrO ₃	114
Figure 5.3:	Measurement of permittivity of Al ₂ O ₃ , MgZrO ₃ and SiO ₃	115
Figure 5.4:	Simulated 3D radiation pattern of parabolic antenna with SPDRA as a feeder (a) 13 GHz, (b) 15 GHz and (c) 18 GHz	116
Figure 5.5:	Simulated and measured radiation pattern of parabolic antenna with SPDRA as a feeder in E- and H-planes at (a) 13 GHz, (b) 15 GHz and (c) 18 GHz	120
Figure 5.6:	Measured and simulated gain of the proposed parabolic antenna using SPDRA as a feeder	121
Figure 5.7:	Simulated 3D radiation pattern of parabolic antenna with SHCDRA as a feeder (a) 13 GHz, (b) 15 GHz and (c) 18 GHz	122
Figure 5.8:	Simulated and measured radiation pattern of parabolic antenna with SHCDRA as a feeder in E- and H-planes at (a) 13 GHz, (b) 15 GHz and (c) 18 GHz	126
Figure 5.9:	Measured and simulated gain of the proposed parabolic antenna using SHCDRA as a feeder	127

LIST OF SYMBOLS

f	focal length
%	Percentage
D	diameter of reflector
d	depth of the reflector
G	gain
A	area of the antenna aperture
λ	wavelength of the radio waves
e_A	effective aperture of the antenna
θ	Angular beamwidth
Q	quality factor
W_e	stored electric energy
W_m	stored magnetic energy
P_{rad}	radiated power
x	x-axis
y	y-axis
z	z-axis
S	maximum acceptable VSWR at the input port of DRA
f_o	Resonant frequency
r	radius
h	height
C	Speed of light
ϵ_r	permittivity
Ω	ohm

f_u	upper resonant frequencies
f_l	lower resonant frequencies
ϵ_o	permittivity of air
V_{dr}	volume of DRs layer
$\tan \delta$	Tangent loss
V_{air}	volume of air
p	distance between the center of holes
s	the diameter of hole
α	filling factor
A_o	area of the hole
A	area of the unit cell
$^{\circ}C$	celcius
R_x	receiver
T_x	transmitter
G_T	gain of AUT
G_S	gain of standard antenna
P_T	power received by tested antenna
P_S	power received by standard antenna
w	width of microstrip line
f_{cen}	center frequency
F/B	front to back ratio
λ_o	wavelength of centre frequency
ϵ_{eff}	effective permittivity
h_t	Total height
η	efficiency of the parabolic antenna

LIST OF ABBREVIATIONS

BW	Bandwidth
VSWR	Voltage Standing Wave Ratio
DRA	Dielectric Resonator Antenna
DR	Dielectric Resonator
TE	Transverse Mode
HCDRA	Half Cylindrical Dielectric Resonator Antenna
HEM	Hybrid Electro Magnetic Mode
3D	Three Dimensions
CDRA	Cylindrical Dielectric Resonator Antenna
RDRA	Rectangular Dielectric Resonator Antenna
UWB	Ultra Wide Band
RDR	Rectangular Dielectric Resonator
DWM	Dielectric Waveguide Model
HDRA	Hemispherical Dielectric Resonator Antenna
CST	Computer Simulation Technology
TM	Telekom Malaysia
MgO	Magnesium oxide
ZrO ₂	Zirconium dioxide
MgZrO ₃	Magnesium zirconium oxide
Al ₂ O ₃	Aluminium oxide (Alumina)
SiO ₂	Silicon dioxide (Silica)
FESEM	Field Emission Scanning Electron Microscope
XRD	X-Ray Diffraction

AUT	Antenna Under Test
PSDC	Penang Skill Development Center
CCTV	Closed-Circuit Television
SHCDRA	Stacked Half Cylindrical Dielectric Resonator Antenna
SCDR	Stacked Cylindrical Dielectric Resonators
SPDRA	Stacked Perforated Dielectric Resonator Antenna

PENYUAP DIELEKTRIK JALUR LEBAR UNTUK ANTENA PARABOLA

K-BAND

ABSTRAK

Parabola antena adalah salah satu alat penting untuk komunikasi jarak jauh seperti hubungan penyiaran radio dan pautan satelit disebabkan oleh gandaan tinggi, pengarahannya yang tinggi dan mempunyai ciri pengendalian kuasa yang tinggi. Di samping itu, penyuaran topi digunakan secara meluas sebagai penyuaran untuk parabola antena kerana paras polarisasi silang yang rendah, unjuran bulatan tepi yang rendah dan pekali pantulan yang rendah. Walau bagaimanapun, penyuaran topi mempunyai lebar jalur yang sempit sehingga 30% yang tidak boleh digunakan dalam aplikasi jalur lebar. Tesis ini menghuraikan pembangunan dan analisis penyuaran jalur lebar antena parabola menggunakan penyuaran penyalun dielektrik (PD). Terdapat dua rekaan antena penyalun dielektrik (APD) jalur lebar menggunakan struktur yang disusun berlapis dengan dua bentuk yang berbeza iaitu silinder dan separuh silinder PD yang dicadangkan dalam kerja ini. PD silinder menggunakan RO4003C, FR4 dan RO6010, manakala PD separuh silinder menggunakan alumina (Al_2O_3), silica (SiO_2) dan magnesium zirkonat (MgZrO_3). APD silinder berlubang (SPDRA) mencapai lebar jalur sebanyak 75.8% dengan purata gandaan 5.65 dBi menggunakan teknik berlubang. Manakala APD separuh silinder berlapis (SHCDRA) mempunyai lebar jalur 61.01% dengan purata gandaan 4.885 dBi, dengan setiap separuh silinder diputar dengan sudut 30° terhadap lapisan berdekatnya. Keputusan pengukuran lebar jalur untuk reka bentuk SPDRA dan SHCDRA menunjukkan keputusan yang munasabah dengan perbezaan 2.7% dan 0.48%, masing-masing perbandingan simulasi. Kedua-dua APD yang dicadangkan dipasang pada pemantul parabola dan

purata gandaan dan lebar pancaran yang dicapai adalah 27.75 dBi, 27.08 dBi dan 4.5° hingga 5.8° dan 4.9° hingga 6.3° , masing-masing. Parametrik analisis telah dijalankan untuk menganalisis dan mengesahkan sifat-sifat antena yang dicadangkan dengan menggunakan perisian Computer Simulation Technology (CST).

WIDEBAND DIELECTRIC FEEDER FOR K-BAND PARABOLIC

ANTENNA

ABSTRACT

Parabolic antennas are one of vital devices for long distance communication such as radio relay links and satellite links due to their high gain, high directivity and high power handling feature. In addition, hat feeder is widely used as a feeder for parabolic antennas due to low cross-polarization level, low sidelobes and low reflection coefficient. However, hat feeder has narrow bandwidth up to 30% which cannot be used in wideband application. This thesis describes the development and analysis of wideband feeder of parabolic antenna using dielectric resonator (DR) feeder. There are two designs of wideband dielectric resonator antenna (DRA) using stacked structure with two different shapes which are cylindrical and half cylindrical DRs are proposed in this work. The cylindrical DRs used RO4003C, FR4 and RO6010, while the half cylindrical DRs used alumina (Al_2O_3), silica (SiO_2) and magnesium zirconate (MgZrO_3). The stacked perforated DRA (SPDRA) achieved bandwidth of 75.8 % with the average gain of 5.65 dBi using perforated techniques, whereas the stacked half cylindrical DRA (SHCDRA) has bandwidth of 61.01% with the average gain range 4.885 dBi, with each of the half cylindrical are rotated by angle of 30° relative to its neighboring layer. The bandwidth measurement results for SPDRA and SHCDRA designs show a reasonable agreement with different of 2.7% and 0.48%, respectively in comparison with simulation. Both of the proposed DRAs were mounted on the parabolic reflector and the average gain and 3 dB beamwidth are achieved 27.75 dBi, 27.08 dBi and 4.5° to 5.8° and 4.9° to 6.3° respectively. A

parametric analysis is carried out to analyze and verify the characteristics of the proposed antennas by using Computer Simulation Technology (CST) software.

CHAPTER ONE

INTRODUCTION

1.1 Introduction

Parabolic antenna is widely used in communication system such as in satellite communication, spacecraft communication, wireless WAN/LAN links for data communication, etc. This is generally due to high directivity, high gain and narrow beamwidth which is suitable for long distance communication. In broadcasting scenario, the compact and economical parabolic antenna, especially in terms of high power transmission and large data is needed. In order to carry the large data, the wide bandwidth antenna is required. As a bandwidth increases, more information per unit of time can pass through the channel. The antenna is considered to be wideband antenna if the operational bandwidth is exceeds 500 MHz or 20% of the center frequency, while the narrow band antenna has less 20% of the center frequency.

There are several types of parabolic antenna with different exciter which is called a feeder. One of them is hat feeder. The hat fed parabolic antenna also used in Malaysia, specifically by Telekom Malaysia Bhd (TM). Currently, TM are using three parabolic antennas which operated a fixed narrow bandwidth (Kildal, 2013) at frequency range of 12.75 GHz – 13.25 GHz (Ku band), 14.4 GHz – 15.35 GHz (Ku band) and 17.7 GHz – 19.7 GHz (both Ku and K bands), respectively. The attention would give to this type of feeder due to its advantage such as low side lobes level, low cross polarization and high illumination efficiency.

The research in the hat antenna design began in 1984, when Per-Simon Kildals designed the primary feeder of the reflector which called the “dipole-disk feed with ring” (Östling, 2013). The research in characterizing feeds for improved

aperture efficiency of the reflector **is** then continued, until the new parabolic antenna with hat feed as a feeder which is called hat antenna in 1986 was introduced. The invention of the hat antenna came from the theoretical formulation of the radiation from the line feeds of the radio telescope in Arecibo in the same year it was introduced. Based on that theory, the corrugated “hat” at the end of the open waveguide can improve radiation efficiency along the outer side of the waveguide. However, the first invention of hat antenna had very narrow bandwidth and couldn’t be used for any application. But, after extensive research especially on the adjustments of its geometry in several years, the hat antenna with good radiation pattern together with low cross-polarization and return loss was invented. Then the first hat antenna was used in a military radio link. The research on the enhancing bandwidth of the hat feed antenna are actively being carried out until now. So far, the bandwidth of the hat feed antenna is around 10% to 33% and it still not enough for carrying larger data (Östling, 2013).

Thus, in this work, the research on the new feeder to replace hat feed was carried out. After preliminary study on the type of antenna which is suitable to integrated with the reflector, the dielectric resonator antenna (DRA) **can** be a potential candidate (Rezaei et al., 2006). It **uses** dielectric material as a resonator that has several drawback such as high cross-polarized (XP) radiation and to difficult integrate with any application platform (Guha & Kumar, 2016). However, it also has many advantages such as small size, light weight, low cost, versatility in their shape e.g. rectangular (Nikkhah & Kishk, 2015), cylindrical (Bhattacharya & Dasgupta, 2016), ring (Feng et al., 2016) and conical (Gharsallah et al., 2015). Furthermore, it also can be excited with various types of feeding mechanism (Singh et al., 2016). In terms of the bandwidth enhancement issue, the idea is by using multiple resonators

by implementing new techniques and new structures. The basic concept is, each of the resonators will contribute to one resonance with a certain frequency band. Then all frequency bands will merge together and contribute to wide frequency band. Finally, the new wideband DRA will be integrated with the reflector for field application.

1.2 Problem Statement

Since 1986 until now, the hat feed parabolic antenna is still being used and the development of the antenna still continue (Östling, 2013). It has several advantages such as low cross-polarization level, low far out sidelobes, low reflection coefficient (Chen et al., 2015) and low blockage as no struts are needed to support it (Motevasselian & Ostling, 2015). Besides that, the corrugations in the brim show a specific impedance which can be used to improve the matching level as well as impedance bandwidth of the antenna. Moreover, the corrugations prevent the waves to propagate in radial direction of the brim, thus forcing the waves to be reflected back to the reflector and leads the spillover efficiency to be improved (Motevasselian & Ostling, 2015). Nowadays, the antenna systems require larger bandwidths than before. In the other words, the desired antenna which can cover many operating band is needed. Thus, the research on the design and development of single wideband parabolic antenna is required. Since the communication technology is growing rapidly with higher data storage transfer, a compact and single wideband parabolic antenna is needed instead of using simultaneously three different parabolic antennas as the current practice. Therefore, a comprehensive research to fulfill this requirement is urgently needed.

There are researches in progress that try to enhance the bandwidth of the hat feeder. The basic structure of hat feeder consists of waveguide, hat and dielectric material inside the hat to support it (Geterud et al., 2013). Originally, it had a bandwidth of 10% (Geterud et al., 2013). Then, the bandwidth was improved to 18% by employing the Chinese hat feed (Yang & Kildal, 1998). In 2007, the bandwidth of hat feed was further improved to 33% by redesign the geometry of the hat feed using generic algorithm optimization (Denstedt et al., 2007). A hat feed without the dielectric material in the hat was presented by (Wei et al., 2011) and as a result, 26% bandwidth was achieved. Based on the history of the effort among the researchers to enhance the bandwidth of the hat feed antenna around the world since 1986 until 2015, it **can be concluded** that the bandwidth was only improved from 10% to 33%. The latest research on hat feed antenna was in 2016. It operates at two bands in the frequency ranges of 38 GHz to 42 GHz and 58 GHz to 62 GHz and the fractional bandwidth is 10% and 6.7%, respectively (Greco et al., 2016). It shows that the research **to** enhancing the bandwidth of parabolic antenna feeder **is ongoing** and new techniques **need** to be explored.

Therefore, the most possible approach to replace the hat feeder is by using dielectric resonator antenna (DRA). It has wider bandwidth which should be able to cover the whole operation frequency of the existing three parabolic antennas. Besides that, it offers higher radiation efficiency and it does not suffer from severe conductor loss (Sarkar et al., 2017), especially at higher frequencies compared to other types of antennas such as microstrip patch antennas, monopole and dipole antennas. In this work, there are two designs of wideband DRAs **proposed** with new techniques and structures. Both of the new DRAs will be **designed** and **simulated** using Computer Simulation Technology (CST). Then, the proposed DRAs will be integrated with

reflector and followed by measurement of bandwidth, radiation pattern and gain to verify the design.

1.3 Research Objectives

The aim of this research is to design and develop wideband parabolic antenna which cover frequency band from 12.75 GHz to 19.7 GHz for wideband application. This thesis focuses on the design and development of wideband parabolic antenna feeder. To accomplish this aim, **specific** objectives have to be achieved. The specific objectives are as follows:

- i. To investigate, design and characterize the DRA with a combination of multiple perforated cylindrical DRs, microstrip fed and rectangular slot in order to increase the operational bandwidth.
- ii. To investigate, design and characterize the DRA with a combination of multiple half cylindrical DRs, microstrip fed and rectangular slot in order to increase the operational bandwidth.
- iii. To integrate the designed wideband DRAs into parabolic antenna as a feeder, while retain the wide bandwidth and high gain characteristics.
- iv. To **analyse** and **compare** the performance of a new DRAs feeding configuration for parabolic antenna in terms of the **bandwidth and gain performance**.

1.4 Organization of The Thesis

This thesis is divided into six chapters. The first chapter is organised in four points: introduction, problem statement, objectives and organization of the thesis.

In Chapter 2, it is made the literature review, which is mainly about the parabolic antenna and dielectric resonator antenna (DRA). It is given special attention to the DRA on the technique to enhance the bandwidth.

Chapter 3 describes the implementation and installation of the DRA to parabolic antenna. The fabrication process to produce DRs from different material composition is explained. The antenna simulation and experiment procedures are described.

Chapter 4 is about explaining the theory of bandwidth enhancement techniques on the proposed DRAs.

Chapter 5 presents the simulation and experimental results for the fabricated prototype of parabolic antenna. An analysis of parametric studies and summary of the obtained results were also discussed.

At last, Chapter 6 is dedicated to the main conclusions of the obtained results, as well as the future work.

CHAPTER TWO

LITERATURE REVIEW

2.1 Introduction

In this chapter, the parabolic antenna, hat feed and DRA is briefly explained. A literature review of DRAs is presented including DRA modes of propagation, geometries, fabrication issues, feeding mechanisms, and several bandwidth enhancement techniques.

2.2 Parabolic Antenna

Reflector antenna has been discovered by Heinrich Hertz since the discovery of electromagnetic wave propagation in 1888. There are several shapes of geometrical configuration such as plane, corner, and curved reflectors (Bakshi & Bakshi, 2009). The most popular shape is paraboloid due to its ability to produce a narrow beam (pencil beam) with high gain. Besides that, it also has very low side lobes and low cross-polarization characteristics in the radiation pattern. It is widely used for point to point communication, wireless WAN/LAN links for data communications, microwave relay links that carry telephone and television signals and spacecraft communication antennas and satellite (Liu et al., 2013).

2.2.1 Parabolic Antenna Operating Principle

A parabolic reflector is formed from a shape of a paraboloid. This shape act as a reflective surface in the antenna that enables waves reflected by the surface and retain their phase relationship. At the transmitter side, the electrical power is supplied through a RF cable to the feeder of the antenna to convert it into the electromagnetic

waves. Then the electromagnetic waves are emitted back towards the reflector into a parallel beam before transmit to the air. Whereas, in the receiving antenna, the incoming electromagnetic waves are bounce off the dish and all the waves are focussed to the feeder of the antenna, which converts them to electrical power which travel through a transmission line to the receiver (Nikkhah & Kishk, 2015).

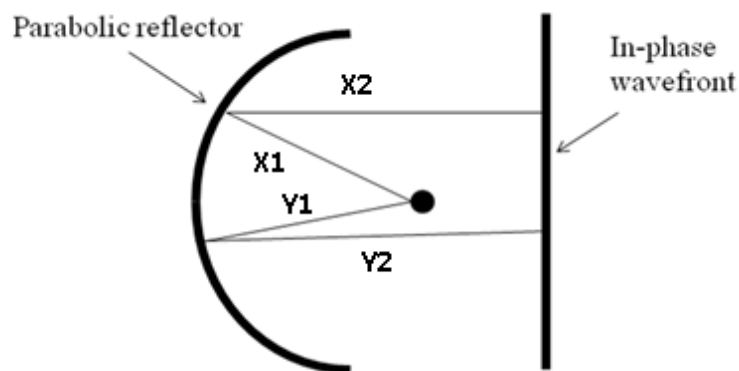


Figure 2.1: A paraboloid enables the wavefronts to combine and not be out of phase

Since the total length $X1 + X2$ is the same as $Y1 + Y2$ as shown in Figure 2.1, the phase integrity of the system is retained. The incoming waves is added at the focal point while outgoing waves are moved in parallel away from the reflector (Nikkhah & Kishk, 2015).

2.2.2 Antenna Feeder

The feeder of the parabolic antenna is typically a low-gain type such as a half-wave dipole. Usually, the feeder was placed at the focal point of reflector (center of the reflector). The focal point is the point where all the reflected waves will be focused or concentrated. The distance of focal point from the center of the reflector

which is called focal length and it is calculated with the Equation (2.1) (Satish Kumar, 2015);

$$f = \frac{D^2}{16d} \quad (2.1)$$

Where,

- f is the focal length
- D is the diameter of the reflector
- d is the depth of the reflector

There are several types of feeds system of parabolic reflector that can be **chosen**. Each of them have their own characteristics that can be used in many application (Nikkhah & Kishk, 2015).

- Front feed – It is the most common type of feed, where the feeder of the antenna placed in front of the reflector at the focus, on the beam axis. The aperture efficiency is around 55 – 60% due to the feeder and the supports block the beam.

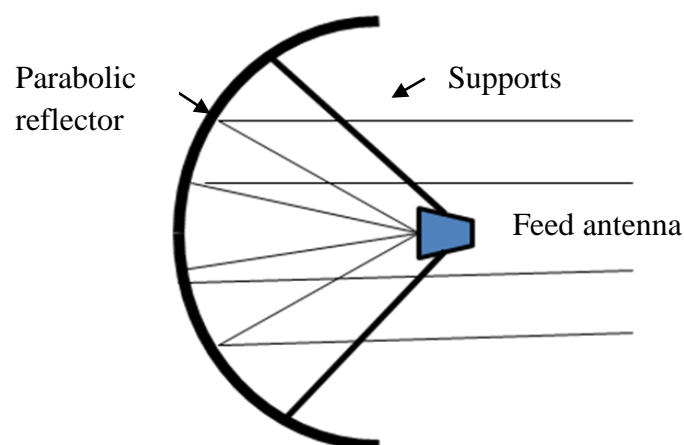


Figure 2.2: Front or axial feed

- ii. Offset axis feed – The feeder of the antenna is located at one side of the reflector since the dish is an asymmetrical segment of a paraboloid. With this feed structure, it does not block the beam.

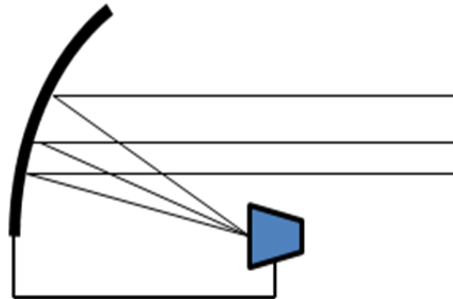


Figure 2.3: Offset axis feed

- iii. Cassegrain – The feeder of the antenna is placed on or behind the reflector and radiates forward while illuminating a convex hyperboloidal secondary reflector at the focus of the reflector. The radio waves from the feeder reflect back off the secondary reflector to the dish, which forms the outgoing beam. The aperture efficiency of this feed structure is around 65 – 70%.

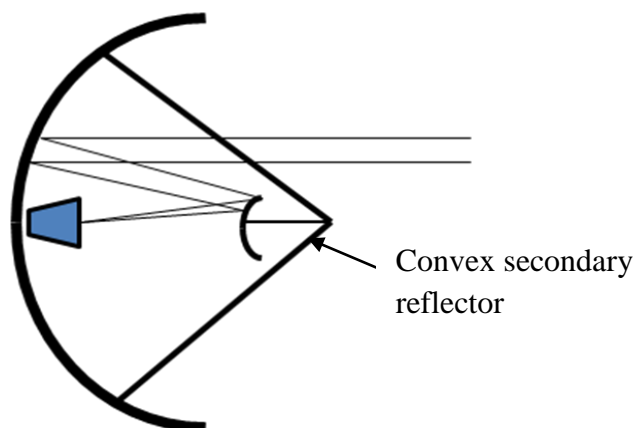


Figure 2.4: Cassegrain feed

- iv. Gregorian – It has a quite similar with the Cassegrain structure except that the secondary reflector is concave shape and the aperture efficiency is over 70%.

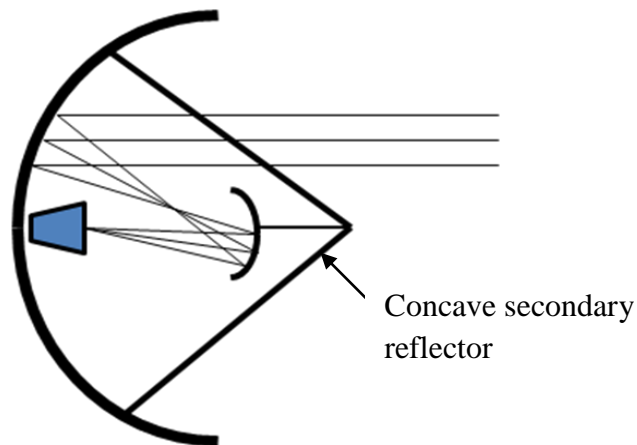


Figure 2.5: Gregorian feed

2.2.2.1 Pyramidal horn antenna

Pyramidal horn antenna is one of the feeder for the parabolic antenna. It can be fed with different exciter such as rectangular, circular waveguides or by a coaxial feed (Ballanis, 1997; Stutzman & Thiele, 2012), but their bandwidth is limited. Numerous coaxial to waveguide probe transitions have been proposed over the years, nearly all of which have less than 35% of Radio Frequency (RF) BWs (Kooi et al., 2003). Research on the printed circuit structures as a exciter for pyramidal horn antenna such as microstrip probe, dipole and patch antennas was carried out in (Caillet et al., 2010; Methfessel & Schmidt, 2010), but the maximum bandwidth achieved is around 30%.

In 2006, Kumar et al. presented new integrated configurations of pyramidal horn antenna excited by suspended square microstrip antenna (MSA) which is placed directly inside the pyramidal horn. It has bandwidth of 185 MHz centered at 3.3 GHz with maximum gain of 11 dBi. The method of the proposed excitation is shown in Figure 2.6 where the pyramidal horn antenna is constructed using suspended square MSA.

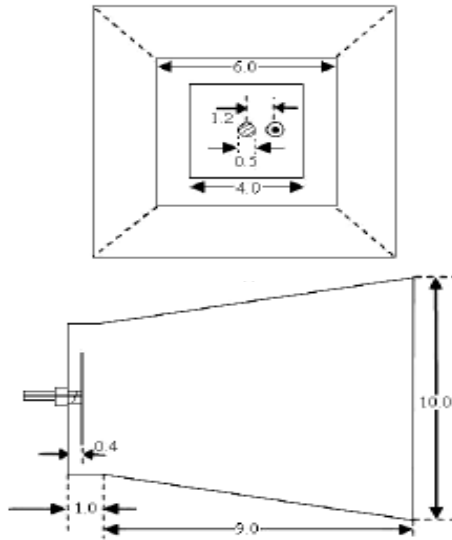


Figure 2.6: Integrated suspended square MSA fed pyramidal horn antenna (unit : cm) (Kumar et al., 2006)

It has been reported in (Shireen et al., 2008), the horn antenna excited by stacked patch antenna with 30% bandwidth is achieved at 94 GHz centered frequency. The excitation method is illustrated in Figure 2.7, showing the configuration of a CPW fed stacked patch with a pyramidal horn.

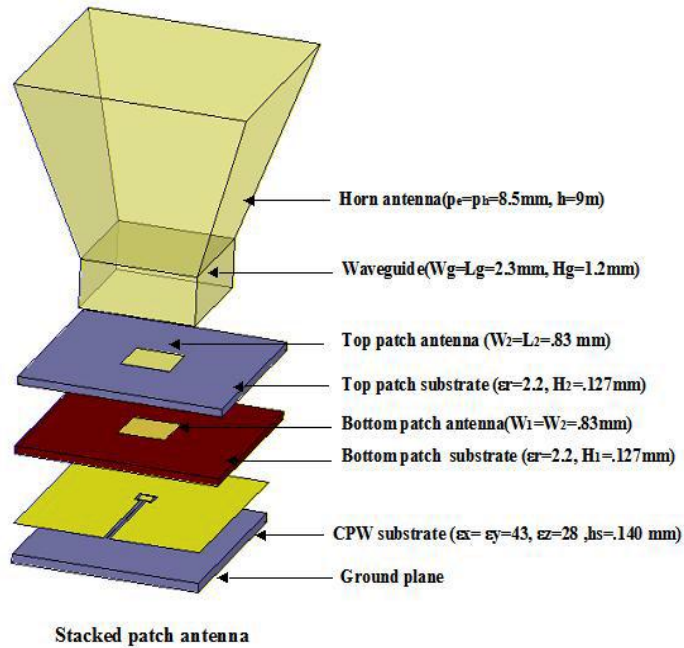


Figure 2.7: Configuration of a stacked patch pyramidal horn antenna (Shireen et al., 2008)

Another method of excitation is reported in (Shireen et al., 2008) by directly placing the planar antenna (i.e., Bow-tie and Vivaldi antennas) on the pyramidal horn as shown in Figure 2.8. Both Bow-tie dipole and Vivaldi slot antennas are achieved wide bandwidth of 18.49 GHz and 24.7 GHz respectively when they are placed inside the horn.

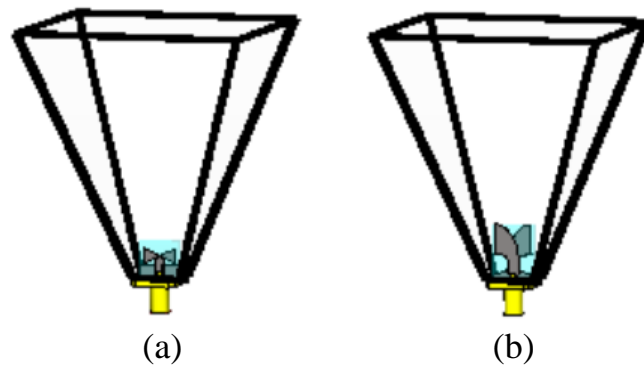


Figure 2.8: Pyramidal horn antenna fed by planar antennas: (a) Bow-tie dipole; (b) Vivaldi (Shireen et al., 2008)

Later in 2011, a new method of excitation for dual-polarized pyramidal horn antenna where microstrip patch is used in order to excite the pyramidal horn was reported in (Shireen et al., 2008). The bandwidth of 4.1% (600MHz) is achieved with the maximum gain of 12.34 dBi. The structure of the excitation method is shown in Figure 2.9.

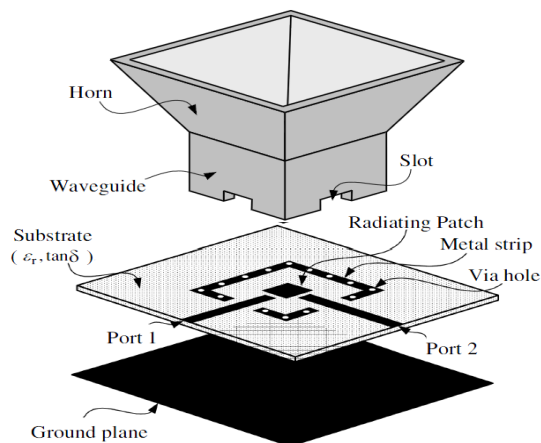


Figure 2.9: Horn antenna excited by microstrip patch configuration (Shireen et al., 2008)

2.2.2.2 Hat feeder

The other type of conventional standard feeder for the parabolic antenna is hat feeder. It was found in 1947, when Cutler proposed the concept of using a self-supported waveguide feed for reflector antennas in order to prevent strut blockage. Later in 1987, Kildal proposed a new self-supported feed, named hat feed that has a corrugated brim surface (the hat) and held up by a piece of dielectric (the head) placed at the end of a waveguide (the neck), as shown in Figure 2.10.

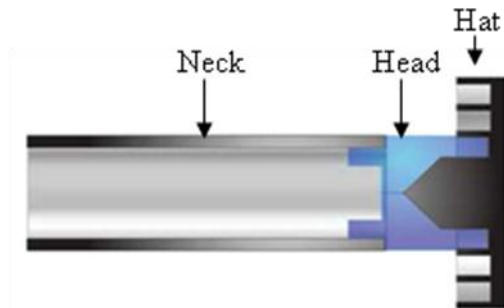


Figure 2.10: Hat feed with corrugated brim (hat), dielectric support (head) and waveguide (neck) (Geterud et al., 2013)

Hat feed has characteristics of excellent side-lobe suppression and its low cross polarization for parabolic antenna feeder (Chen et al., 2015). The 2D structure of hat feeder with and without corrugation are shown in Figure 2.11. When the smooth metal surface without corrugation is used for the hat, the z component of E-field can propagate along the hat surface will cause the field illumination high on the edge of the reflector and develop the far-out sidelobes' level as shown in Figure 2.11(a). The corrugation on the hat used to stop the propagation of the z component E-field and also decrease the far-out sidelobe level, as shown in Figure 2.11(b).

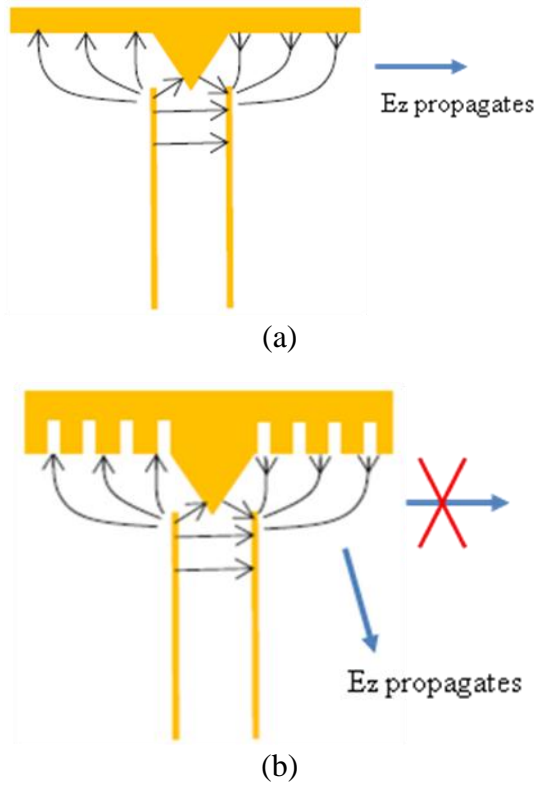


Figure 2.11: The working principle (a) no corrugation introduced on hat, (b) corrugation introduced on hat (Chen et al., 2015)

However, the hat feed has a narrow bandwidth. Since 1986, the research to enhance the bandwidth of the hat feed still carrying on until today (Östling, 2013). Table 2.1 summarizes some efforts to enhance bandwidth of the hat feed.

Table 2.1: Summary of measured hat feed with enhanced impedance bandwidth

Bandwidth (%)	Frequency range (GHz)	References
10	n/a	(Kildal & Yang, 1997)
18	n/a	(Yang & Kildal, 1998)
33	n/a	(Denstedt et al., 2007)
26	n/a	(Wei et al., 2011)
26	n/a	(Yang & Wei, 2011)
29.7	10.75-14.5	(Geterud et al., 2013)
10 and 6.7	38- 42 and 58- 62	(Greco et al., 2016)
4.8 and 3.3	20.2- 21.2 and 30- 31	(Yavuz et al., 2016)

2.2.3 Gain and Efficiency

In general, the antenna gain is the ratio of the power received by the antenna under test (AUT) to the power received by an isotropic antenna. But, for the gain of a parabolic antenna is calculated using the Equation (2.2) (Satish Kumar, 2015),

$$G = 10\log_{10} \frac{4\pi A}{\lambda^2} e_A = 10\log_{10} \frac{\pi^2 d^2}{\lambda^2} e_A \quad (2.2)$$

where:

- A is the area of the antenna aperture.
- d is the diameter of the parabolic reflector
- λ is the wavelength of the radio waves.
- e_A is the effective aperture of the antenna.

The e_A takes into account for many losses that can reduce the gain of the parabolic antenna from the maximum. The major factors reducing the e_A in parabolic antennas are (Baars & Swenson, 2008):

- Illumination taper
- Spillover loss
- Focal point error
- Blockage by the feeder
- Blockage by the supporting structures
- Imperfection in parabolic surface
- Feedline loss

2.2.4 Beamwidth

The angular beamwidth of transmit antennas is calculated by the half power beam width (HPBW), which is the θ between two point antenna radiation pattern at which the power drops half from the maximum value. The θ can be determine using Equation (2.3) (Satish Kumar, 2015):

$$\theta = \frac{70\lambda}{d} \quad (2.3)$$

where d is the diameter of the reflector.

The relation between gain and beam is in Equation (2.4) (Satish Kumar, 2015)

$$G = 10\log_{10}\left(\frac{70\pi}{\theta}\right)e_A \quad (2.4)$$

2.3 Dielectric Resonator Antennas

DRAs have attractive antenna features and have many advantages compare to the other antennas. These advantages are small size, low conductor losses, low cost, high radiation efficiency and a wide variety of feed mechanisms. DRA's are available in various shapes and sizes as shown in Figure 2.12 (Mongia and Bhartia, 2007, Petosa et al., 1998). DRA also can be used in various applications such as video conferencing, direct digital broadcast, wireless communications and radar applications as they require wide bandwidth. The DRA is achieved wideband with low values of ϵ_r , as it is known that the bandwidth of the antenna is inversely proportional to the ϵ_r (Pandiya et al., 2016).

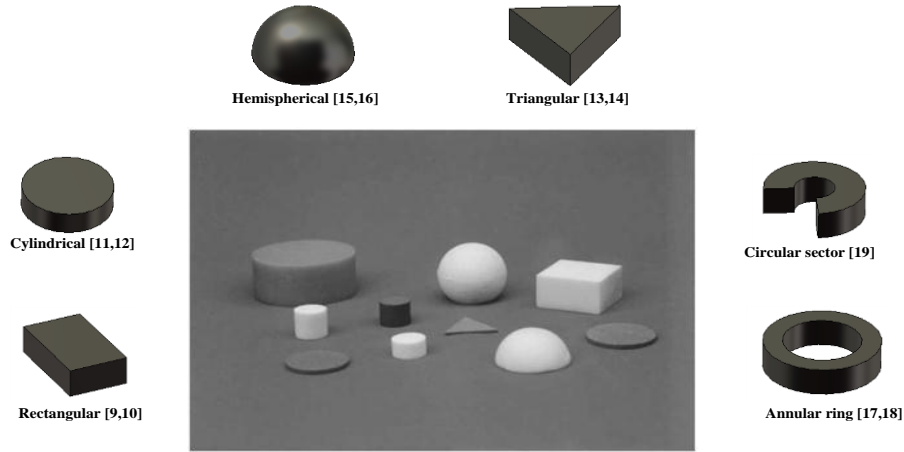


Figure 2.12: Various DR geometries (Luk & Leung, 2003)

2.4 Characteristics of DR

2.4.1 Dielectric Permittivity

The ϵ_r is the ratio of the permittivity of the dielectric material to permittivity of free space. The main characteristic of a dielectric material is, it can support an electric field and dissipate least energy in the form of heat. The lower dielectric loss ($\tan \delta$), the more effective a dielectric material is.

2.4.2 Quality Factor

The Q factor is defined as a relation between the store energy in the reactive field and radiated power of the antenna (Gustafsson & Nordebo, 2006),

$$Q = \frac{2\omega(W_e W_m)}{P_{rad}} \quad (2.5)$$

where W_e , W_m and P_{rad} are the stored electric energy, stored magnetic energy and radiated power, respectively.

2.4.3 Bandwidth

In general, all the antennas have a limited operating bandwidth and it can be estimated using Equation (2.6):

$$\text{Bandwidth} = \frac{S-1}{Q\sqrt{S}} \quad (2.6)$$

where S is the maximum acceptable VSWR at the input port of DRA.

2.4.4 DRA Fabrication Issues

When evaluating the performance of the DRA, it may confront from the following issues (Alam, 2012):

- Fabrication tolerance of DRA geometry and feeder network.
- DRA cutting accuracies.
- Variation of permittivity values.
- Usage of adhesive materials to glue DRAs to the ground planes.
- Existing of unwanted air gaps.

2.5 Cylindrical DRA

Due to less complicated in fabrication and cheaper in cost compared to other shapes, the cylindrical shaped DRA is the most commonly used in practical application. Cylindrical DRA (CDRA) gives design flexibility for the control of the BW and the resonant frequency, where both Q -factor and resonant frequency rely on the given ratio of radius to height, a/h as illustrated in Figure 2.13. Figure 2.13 shows a dielectric cylinder of height h , radius a and ϵ_r is placed on a fixed ground plane.

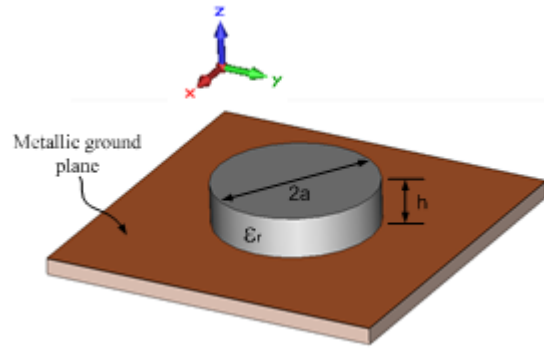


Figure 2.13: Cylindrical DRA geometry on metallic ground plane.

The CDRA has three types of modes: $TE_{n_{pm}+\delta}$, $TM_{n_{pm}+\delta}$ and the $HEM_{n_{pm}+\delta}$ which are transverse electric, transverse magnetic and hybrid modes, respectively (Drossos et al., 1996; Mongia & Bhartia, 1994). The indices n , p , m stands for the number of full-period field variations in the azimuth, the radial and the axial direction respectively. The index δ value is between 0 and 1, approaching 1 for high ϵ_r . Figure 2.14 and Figure 2.15 illustrate the fields distribution of two low order modes, $TM_{01\delta}$ and $HEM_{11\delta}$, respectively. These two modes have an equatorial plane of symmetry that acts like an electric wall.

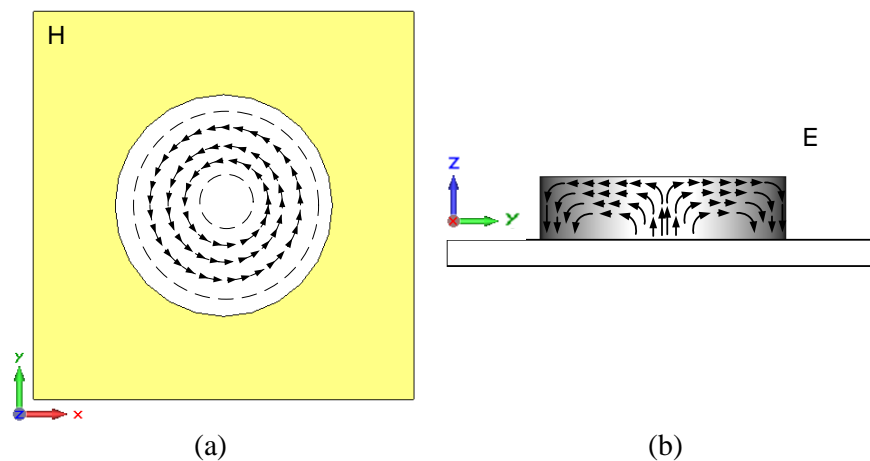


Figure 2.14: Field distribution of the $TM_{01\delta}$ mode: (a) DRA field H_x and H_y at $z = 0$; (b) DRA fields E_y and E_z at $x = 0$ (Kajfez et al., 1984).

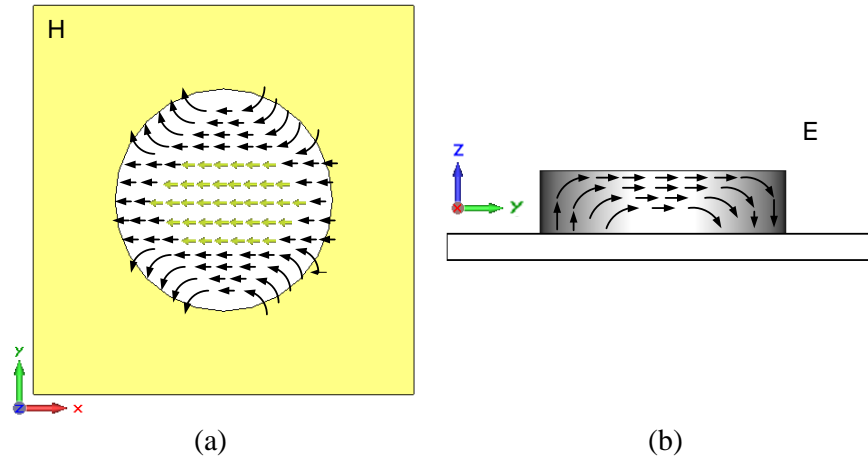


Figure 2.15: Field distribution of $HEM_{11\delta}$ mode: (a) DRA field H_x and H_y at $z = 0$; (b) DRA fields E_y and E_z at $x = 0$ (Kajfez et al., 1984).

From Figure 2.14 and Figure 2.15, it can be observed that the H-field distribution inside the DRA is of the same distribution as the one generated by a monopole antenna. In this particular case, the DRA $TM_{01\delta}$ mode can be excited by a probe situated at the centre of the DRA. The radiation patterns produced by these modes can easily be predicted based on the field distribution inside the DRA.

There are various types of feeder such as probes, microstrip, slot-microstrip slot-waveguide, slot image and image wave guide can be used to excite CDRA as illustrated in Figure 2.16. The way using the feeding technique and the location of the feeding components are very essential in determining which modes of antenna have been excited. It also alters the resonant frequency, Q factor, input impedance and radiation characteristics of isolated CDRA.

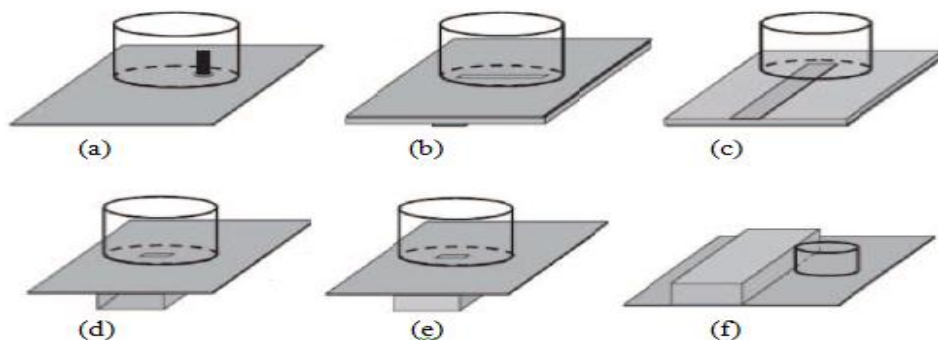


Figure 2.16: Different excitation techniques of DRA: (a) Coaxial probe, (b) Slot-microstrip, (c) Microstrip, (d) Slot-waveguide, (e) Slot-image and (f) Image guide (Singh et al., 2016)

Feeding methods used in the design for coupling purpose of DRA greatly affect the design parameter and hence the design equation. The theoretical formula of cylindrical DRA for resonant frequency can be calculated by Equation (2.7) (Benomar et al., 2011).

$$f_0 = \frac{2.208 \times c}{2\pi h \sqrt{\epsilon_{eff} + 1}} \left[1 + 0.7013 \left(\frac{r}{h} \right) - 0.002713 \left(\frac{r}{h} \right)^2 \right] \quad (2.7)$$

Where r and h are the radius and the height of DR, respectively.

2.6 Half Cylindrical DRA

A half cylindrical DRA (HCDRA) can give multiple radiating modes. If it is properly excited, impedance bands corresponding to those modes which are similar in terms of radiation properties can be merged to have wideband DRA (Praveen et al., 2006). In 1989 Mongia proposed a half-split cylindrical DRA with $TE_{01\delta}$ mode for wide bandwidth applications. Later, Mongia et.al. proposed the slot coupling to excite the $TE_{01\delta}$ mode in half-split cylindrical DRA and about 10% bandwidth experimentally with broadside radiation pattern have been achieved (Chaudhary et al., 2013).

The performance of the cylindrical DRA when half of its volume was removed was studied in (Tam & Murch, 1997). It was found that the DRA still have same performance instead of its half volume removal. In this work, half of the DR was reduced by using a thin metal plate was placed perpendicular to the ground plane. The metal plate behaves as a shorting plane for the E-field and allows a part of the DRA to be discarded if certain field symmetry exists. The symmetrical electric fields lines along the line AB is shown in Figure 2.17. As the field distribution

remains the same, the resonant frequency also remain the same and therefore the volume of the DRA is effectively reduced by half. This structure is referred as the HCDRA and the impedance characteristics of the DRA will change from the conventional DRA since the radiating surface has also been cut by half. Therefore, the position and length of the probe need to be adjusted to have a good impedance match for the half volume DR (Tam & Murch, 1997).

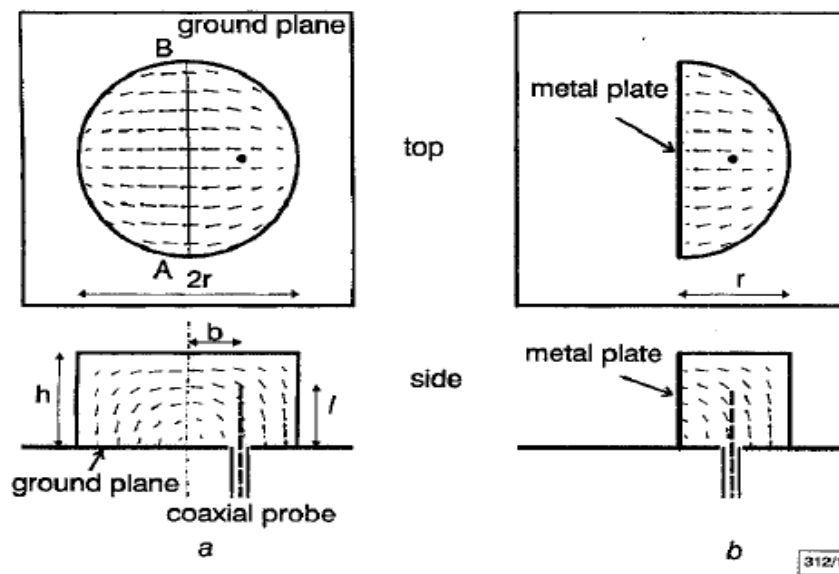


Figure 2.17: Geometry of (a) Cylindrical and (b) Half-cylindrical DRA (Tam & Murch, 1997)

Another technique to reduce half volume of cylindrical and rectangular DRs using conducting plates was studied in term of the resonant frequency, impedance, field distribution and radiation pattern. The DRs was excited by a probe and it was placed on a radius halfway to the outer edge the cylindrical in such a position as to excite the $HEM_{11\delta}$ mode. With the conducting plane is fixed at the center of cylindrical, the symmetry of the field lines is generated and the resonant mode is retained. A similar approach is implemented to the rectangular DRA that operates in the TE mode as shown in Figure 2.18(b). The coaxial probe was placed perpendicular to the ground plane at the center of half rectangular DR, and the

position and length of the probe was adjusted to maintain the correct impedance of half rectangular DRA (O’Keefe et al., 2002).

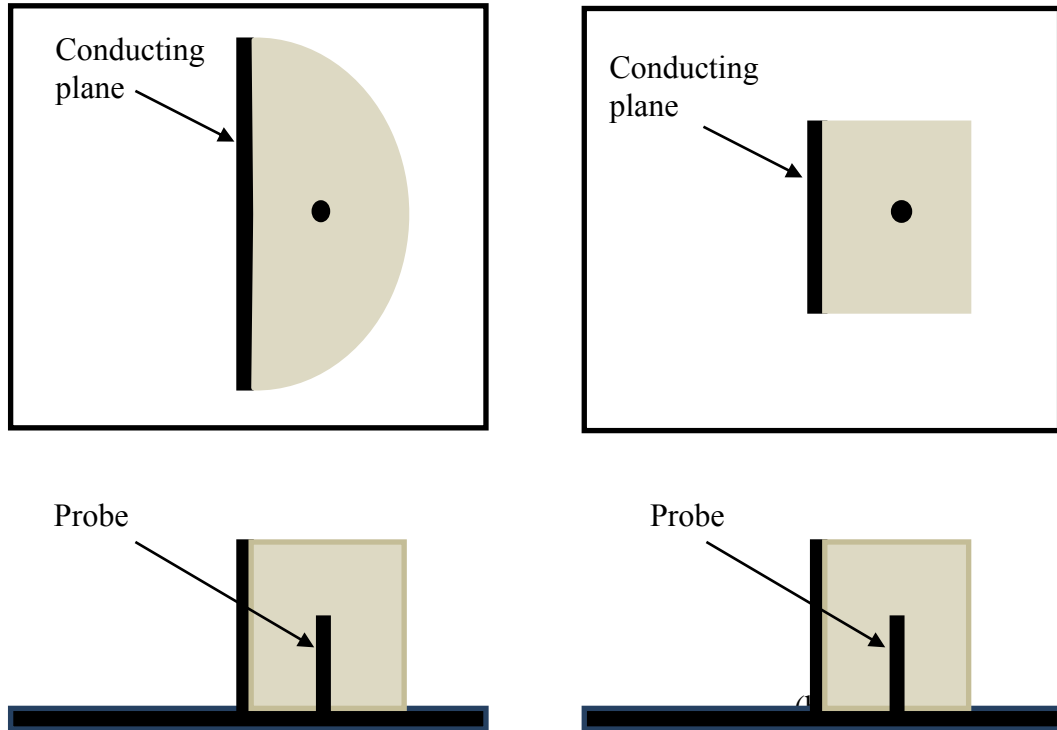


Figure 2.18: Structure of the DRA (a) half cylinder and (b) half rectangular (O’Keefe et al., 2002)

From the experiment it is found that the half DRAs are lower in volume and have a more directional radiation pattern compared to the solid cylindrical and rectangular. Between half rectangular and half cylinder, the half-rectangular DR has a poorer F/B ratio and high rear lobe is due to the imperfect shielding served by the metal divider (O’Keefe et al., 2002).

A half cylindrical DR with high permittivity ($\epsilon_r = 69$) of ceramic material with 50Ω microstrip line as an exciter was studied in (Praveen et al., 2006) as shown in Figure 2.19. It is found that, it has a wide and stable radiation over a matching band. In this work, the wide bandwidth is obtained by properly adjusted the feed position to merge all the multiple resonances